

Single multimode fibre for in vivo light-field-encoded endoscopic imaging

Received: 23 June 2022

Accepted: 23 May 2023

Published online: 3 July 2023

 Check for updates

Zhong Wen^{1,2}, Zhenyu Dong^{1,2}, Qilin Deng^{1,2}, Chenlei Pang², Clemens F. Kaminski³, Xiaorong Xu², Huihui Yan⁴, Liqiang Wang^{1,2}, Songguo Liu², Jianbin Tang⁵, Wei Chen⁶, Xu Liu^{1,2,7,8} & Qing Yang^{1,2,7,8}

Super-resolution microscopy is typically not applicable to in situ imaging through a narrow channel due to the requirement for complex optics. Although multimode fibres (MMFs) have emerged as a potential platform for cost-effective and precise endoscopic imaging, they suffer from extreme sensitivity to bending and other external conditions. Here we demonstrate imaging through a single thin MMF for in vivo light-field encoded imaging with subcellular resolution. We refer to the technique as spatial-frequency tracking adaptive beacon light-field-encoded (STABLE) endoscopy. Spatial-frequency beacon tracking provides up to 1 kHz disorder tracking frequency, thus ensuring stable imaging through long-haul MMFs under fibre bending and various operating conditions. The full-vector modulation and fluorescence emission difference are combined to enhance the imaging signal-to-noise ratio and achieve a subdiffraction resolution of 250 nm. We integrate STABLE in a white-light endoscope and demonstrate cross-scale imaging in a bronchus model and in vivo imaging in mice models. The high-resolution and resilience to observation in a minimally invasive manner paves the way to the expansion of MMF in endoscopy to the study of disease mechanisms in biomedical sciences and clinical studies.

One of the ultimate dreams of endoscopists would be real-time high-resolution endoscopy that combines in vivo imaging and therapeutic intervention, resulting in an endoscopic diagnosis that matches an in vitro pathological diagnosis^{1,2}. Considerable progress has recently been made in endoscopy. Endocytoscopy, confocal laser endomicroscopy and other techniques have been developed to enable in vivo cellular imaging^{3–8}. Meanwhile, super-resolution microscopy enables spatial resolution at much smaller scales than the subcellular level, leading to breakthroughs in the fields of biology and life sciences^{9–13}.

However, super-resolution microscopy often requires cumbersome optics and is thus challenging to implement in a narrow channel. In fact, one critical missing ability is to conduct robust in vivo nano-endoscopy, which is yet to be satisfactorily established. One promising strategy is to employ thin multimode fibres (MMFs) as minimally invasive probes using wavefront shaping. The mode density of MMFs is 2–3 orders of magnitude higher than those of traditional endoscopes of the same diameter^{14–30}, but this technology has two critical limitations: the operational inflexibility due to the strong transmission dependence

¹State Key Laboratory of Extreme Photonics and Instrumentation, College of Optical Science and Engineering; International Research Center for Advanced Photonics, Zhejiang University, Hangzhou, China. ²Research Center for Humanoid Sensing, Zhejiang Lab, Hangzhou, China. ³Department of Chemical Engineering and Biotechnology, University of Cambridge, Cambridge, UK. ⁴Department of Gastroenterology, The Second Affiliated Hospital, Zhejiang University School of Medicine, Hangzhou, China. ⁵Key Laboratory of Smart Biomaterials of Zhejiang Province, College of Chemical and Biological Engineering, Zhejiang University, Hangzhou, China. ⁶Key Laboratory for Biomedical Engineering of the Ministry of Education, College of Biomedical Engineering and Instrument Science, Zhejiang University, Hangzhou, China. ⁷Collaborative Innovation Center of Extreme Optics, Shanxi University, Taiyuan, China. ⁸ZJU-Hangzhou Global Scientific and Technological Innovation Center, Hangzhou, China. ✉e-mail: liuxu@zju.edu.cn; qingyang@zju.edu.cn

on the fibre's configuration^{20–22} and the diffraction-limited resolution due to limited numerical aperture (NA)¹⁵. The dynamic change and interference between different deformation states of the fibre is a major obstacle to rapid disorder measurement, tracking and image correction. Many past studies have attempted to compensate for the effect of fibre's dynamic movement with strategies that mainly fall into two categories (Supplementary Table 1): tracking based on slow spatial area detection^{23,24,31–33} or no tracking^{20,21,25,28}. It is challenging to conduct imaging under bending and various operating conditions. On the other hand, complex engineering of the fibre's distal facet is often required^{23,24,31–33}. With these accumulating challenges, techniques have not yet demonstrated sufficiently high-resolution imaging under practical operational conditions due to the lack of fast tracking and super-resolution methods.

Here we propose an MMF-based spatial-frequency tracking adaptive beacon light-field encoded (STABLE) endoscope imaging (Fig. 1). The system can be used in ultrathin and ultralong channels and improves the resolution to a subdiffraction-limited value of 250 nm ($\lambda/3NA$) with high stability and robustness against the movement and deformation of the probe. STABLE endoscopy and self-designed white-light endoscopy (WLE) are integrated to achieve centimetre-to-nanometre cross-scale imaging of various samples inside narrow channels. The WLE can provide a 120° wide field-of-view (FOV) to locate areas of interests. STABLE endoscopy can provide sub-cellular resolution for precise analysis. In our experiments we apply the STABLE endoscopy to a number of clinical samples, including test targets, pathological samples, nanomaterials and living mice. Our study illustrates the potential to greatly expand the flexibility of STABLE endoscopy, making a substantial leap towards applications in the life sciences, biology, industrial inspection, as well as clinical diagnoses.

Principle of STABLE

Perturbations and coupling between spatial or polarization modes—or both—are inevitable and non-negligible, and are thus obstacles in the way of using MMF imaging for in vivo applications^{34–36}. They have limited the MMF imaging applications under practical movement for approximately decades. We introduce the STABLE concept to eliminate the influence of unpredictable couplings and fluctuations (Fig. 1a). Taking endoscopy applications as an example, eliminating the influence of the dynamic changes requires searching the transmission matrix (TM) based on the light reflection of the closed space immediately during endoscope movement. Tracking was previously based on speckle measurement of the whole image with an engineered distal facet^{23,24,31–33}, and several minutes were required to find the correct TM after the change²⁴ (Supplementary Table 1).

In STABLE, we designed a full-vector modulation (FVM) incident wavefront that focuses the distal-end Fresnel reflection light on a single-pixel detector in the spatial-frequency domain (that is, the Fourier plane of the proximal facet of the fibre), forming the spatial-frequency beacon (Fig. 1b, left). The beacon transfers from spatial speckle tracking to single-pixel spatial-frequency beacon tracking. Its strength reflects the correlation between the current bending states and the pre-calibrated TMs. By analysing the simulation of light propagation in the fibre, and the relationship between the reflection light and spatial-frequency beacon, we find that the spatial-frequency beacon intensity detected by the single-pixel detector is directly related to the chaotic phase, polarization and amplitude, all of which are relative changes that accompanies fibre deformation (Supplementary Fig. 3). The correct fibre state can be found only when the intensity value is at its maximum. It is therefore possible to search for the correct TM under deformation by tracking the beacon.

STABLE is a highly dimensionality reduction single-pixel tracking method that takes advantage of the fact that the MMF is a radial cylindrically symmetric waveguide. Through simulations and experiments we found that the spatial-frequency beacon intensity maintains a high

intensity (that is, more than half of the initial value, Supplementary Figs. 4–7 and Supplementary Note 1) under rotation, limited translation and small twist of the fibres (Fig. 2a). Measuring and updating the TM can be skipped in these scenarios (Supplementary Video 3). This compresses the problem to a much lower order (Fig. 1c). We can therefore just pre-measure the TM under different bending curvature and build a relative complete database for calibration. Furthermore, the database searching process based on single-pixel beacon tracking could eliminate the iteration of TM, which is always the bottleneck in speeding the compensation. The time taken to find the correct TM from a database (about 20–100 states) is in the order of 10^{-3} s. The search speed is enhanced by a factor of 10^4 compared with the spatial domain tracking (Fig. 2b,c, Supplementary Table 1, Supplementary Video 4 and Supplementary Fig. 10).

STABLE process

STABLE can be divided into database creation and imaging recovery processes (Supplementary Fig. 8). The experimental system is shown in Supplementary Fig. 17.

In the creation of the STABLE database, customized for each endoscopist, we pre-measured and created a highly effective database containing a set of TMs and reflection matrices (RMs) under different bending states (Supplementary Fig. 8). The spatial-frequency beacon is generated using RMs. It describes the linear input–output response of an MMF at the same port. The RM can be obtained using the Onsager reciprocity relationship and end-facet Fresnel reflection³⁷, as shown in equation (1):

$$RM = T^T F T \quad (1)$$

Here, T^T represents the transpose of TM and F is the end-facet Fresnel reflection matrix.

Dual feedback loops are introduced into the STABLE imaging process. The spatial-frequency beacon provides fast encoded feedback in the inner loop to track the deformation state (loop 1 in Supplementary Fig. 8b). The imaging sharpness acts as encoded feedback in the outer loop to track the focus plane (loop 2 in Supplementary Fig. 8b). Their cooperation enables highly stable imaging. The system includes an optical module, a probe and an electrical module (Fig. 1d). The transfer functions of loops 1 and 2 are as follows:

$$T^{t+1} = T^t + (1 - G(T^t))T^t \text{ for loop1} \quad (2)$$

$$H^{t+1} = H^t + (1 - O(H^t))H^t \text{ for loop2} \quad (3)$$

Here, G and O represent the normalized intensity of the spatial-frequency beacon and image sharpness, respectively; $H = \exp(-id\sqrt{k_0^2 + l^2 + k^2})$ is the propagation factor, which is a quadratic phase resulting in imaging plane axial movement; k and l are positions in Fourier space; d is propagation distance; $k_0 = 2\pi/\lambda$ is the wavenumber in free space; and t is the index of retrieval.

Under the framework of STABLE, the key to high-quality volumetric imaging lies in the efficient generation of beacons and the formation of high-signal-to-noise ratio (SNR) scanning points in three-dimensional space. Volumetric imaging is difficult with the conventional MMF imaging method due to the extreme complexity in alleviating mode and polarization dispersion during the generation of the TM stack at different axial distances (Supplementary Fig. 20). In this study, the mode dispersion, polarization-mode dispersion and mode-dependent losses occurring along the fibre length are resolved via FVM (equation (4)):

$$\psi_{in}^{u,v} = T^{tik} H \psi_{out}^{k,l} \quad (4)$$

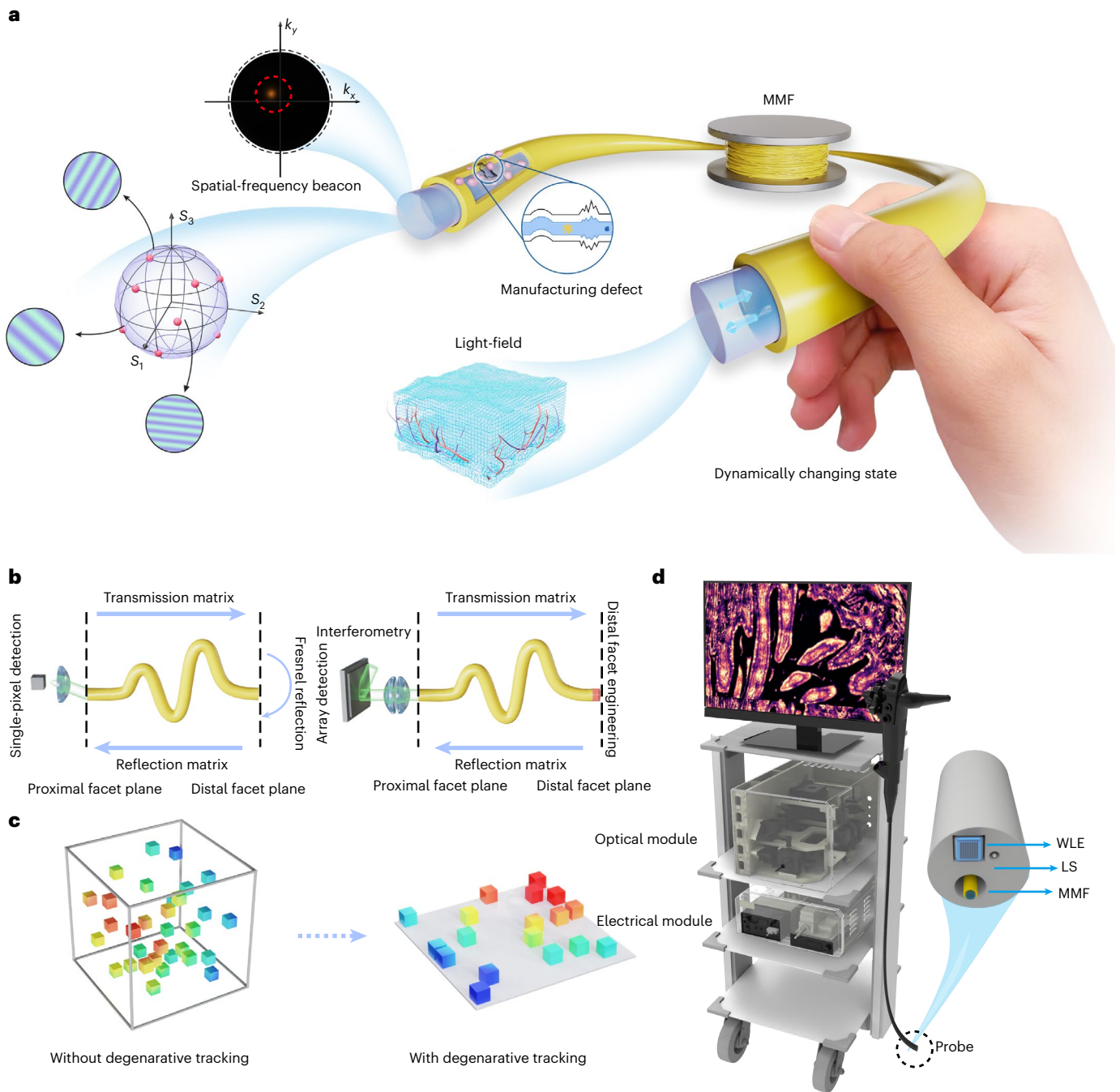


Fig. 1 | Principle of the STABLE system. a, STABLE can detect and track disorders in the MMFs introduced by practical movements and manufacturing defects, thus retaining high-SNR imaging. The input light is composed of all spatial-frequency modes in designed polarization states, which are spread over the Poincaré sphere. S_1 to S_3 represent the three polarization components. The spatial-frequency beacon is located at the Fourier plane of the fibre proximal end. k_x and k_y are positions in Fourier space. **b**, Diagram of spatial-frequency beacon (left) and conventional spatial speckle (right) monitoring. In spatial-frequency beacon monitoring, the modulated wavefront with designed polarization is incident into the MMF, reflected by the distal facet of the fibre, and then returned

to the proximal facet again, focusing on a single pixel in the spatial-frequency domain as spatial-frequency beacon. In conventional monitoring, the modulated wavefront with the same polarization is incident to the MMF, reflected by distal facet engineered, and then returned to the proximal facet again, imaging on array detection. **c**, Dimension reduction retrieval concept map. STABLE is a highly compressive method that takes advantage of the fact that the MMF is a radial cylindrically symmetric waveguide. This compresses the problem from a high-order problem to a much lower-order problem. **d**, Endoscope prototype. The black dotted line shows the probe. WLE, white-light endoscopy; LS, light source of WLE; MMF, multimode fibre.

where T^{Tik} is the Tikhonov regularization of T ; $\psi_{in}^{\mu,\nu}$ is the mode distribution of the input field; $\psi_{out}^{k,l}$ is the distribution of the output field; and μ, ν and k, l represent the two-dimensional spatial-frequency factors at the two ends of the fibre.

Simulations and experiments indicate that FVM can convert the MMF function to a highly efficient programmable full-vector holographic device (Supplementary Fig. 20g–j and Supplementary Note 4). A high-contrast full-vector TM stack can therefore be obtained with

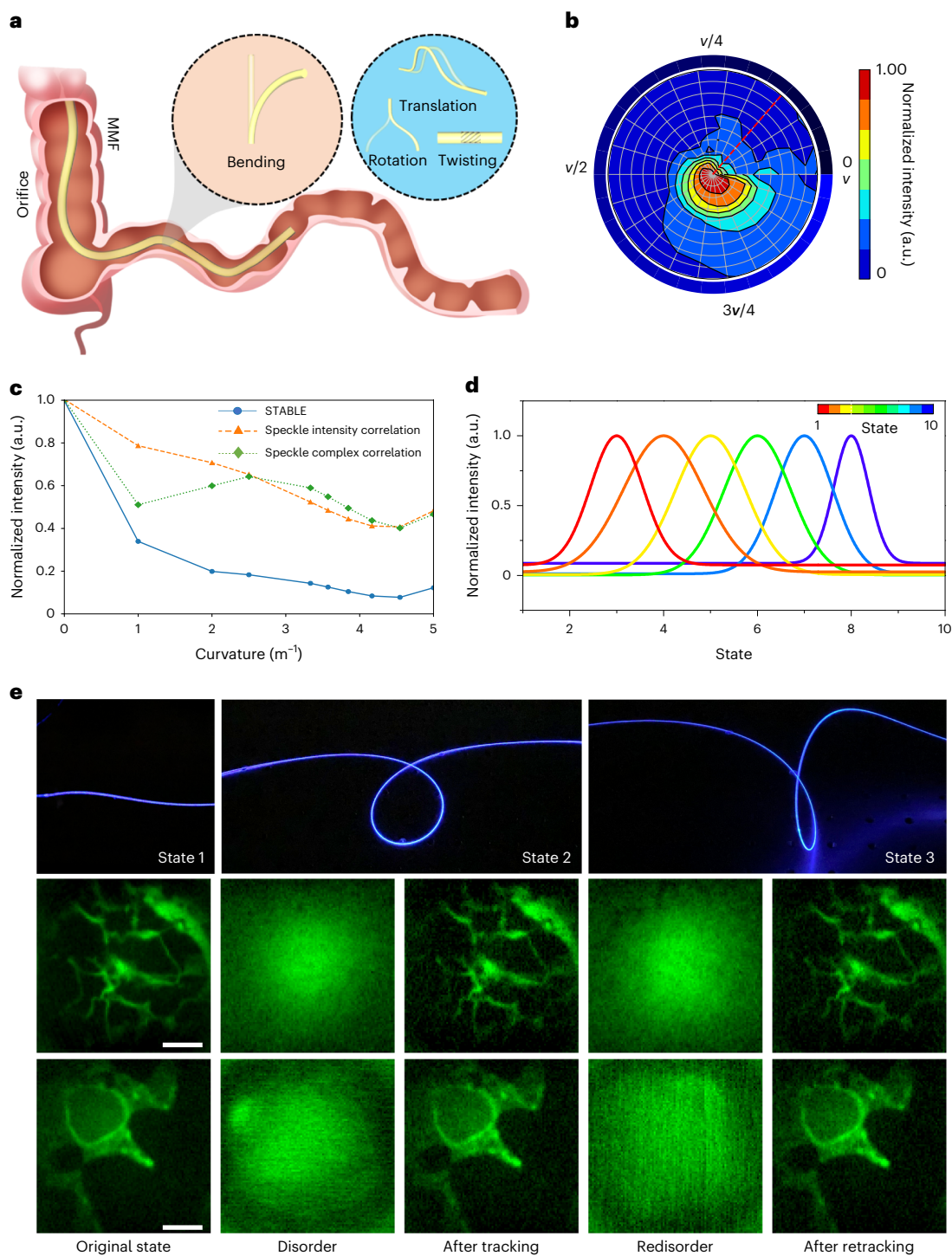


Fig. 2 | Deformation disorder tracking and compensation in MMF imaging.

a, Types of fibre deformations. Orange circle, bending deformation; blue circle, other three deformations (translation of a fixed curvature fibre, rotation around a central axis and twisting deformation). **b**, Spatial-frequency beacon intensity variation with bending at different locations in the spatial-frequency domain. The angular coordinate is the spatial-frequency, and ν is the maximum spatial-frequency of the MMF. The radial coordinate represents curvature from 0 m^{-1} to 5 m^{-1} . The normalized intensity represents the ratio of spatial-frequency

beacon intensity in straight state to that in different curvature. **c**, The feedback of different probes under bending. The location of the spatial-frequency beacon is indicated by the red dashed line in **b**. **d**, Retrieval of the bending state based on spatial-frequency beacon tracking. **e**, The state change and imaging recovery. The first row represents different fibre states, whereas the second and third rows represent the tracking and recovery processes of MMF imaging of atherosclerotic and lung pathology slides under the corresponding states, respectively. Scale bars, $25 \mu\text{m}$.

a single measurement. In practical applications, the combination of TM within the acquired stack with image sharpness O in loop 2 can fix the preferable imaging planes within the depth range for stable volumetric imaging.

Furthermore, super-resolution imaging can be obtained by using FVM to perform a spatial-frequency shift super-resolution method (here, differential fluorescence microscopy) on the sample. Conventional differential fluorescence microscopy loses both resolution and

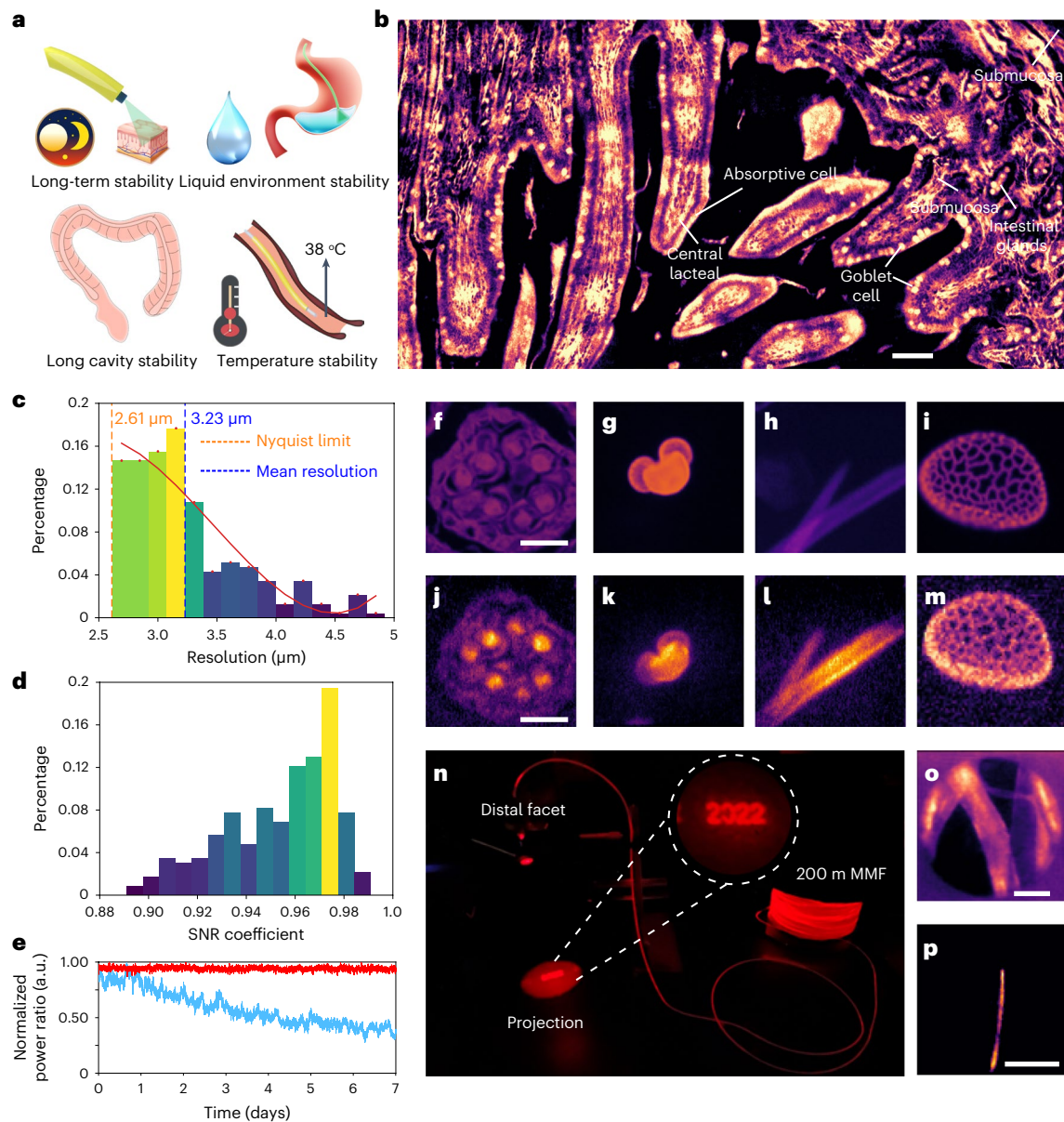


Fig. 3 | Complex environments tracking and compensation in MMF imaging. **a**, Concept diagram of endoscopy in complex environment (long-term, liquid, long cavity, temperature variations). **b**, Image of a sheep's small intestine captured via MMF endoscopy. The types of cells are annotated on the image. The images are captured at different times over 5 days and can be stitched to a large FOV image without distortion, indicating the long-term stability of the system. This image corresponds to the dashed box in Supplementary Fig. 13a. Scale bar, 150 μm . **c**, Resolution of each image before stitching. The horizontal axis indicates the resolution of the images, whereas the vertical axis represents the percentage

of the total number of images. **d**, The SNR of each image before stitching. The vertical axis indicates the percentage of the total number of images, whereas the horizontal axis represents the SNR of the images. **e**, Focus intensity variation during a long period of time. **f–i**, Wide-field microscopic images of broad bean anther (**f**), onion pollen (**g**), basswood segregation (**h**) and lily pollen samples (**i**). Scale bar, 40 μm . **j–m**, The corresponding 50 m MMF images of the samples in **f–i** placed underwater. Scale bar, 40 μm . **n**, High-contrast projection through 200 m MMF. **o**, Imaging of fluorescent lens paper with 200 m MMF. Scale bar, 15 μm . **p**, Imaging of CdSe nanowire with 200 m MMF. Scale bar, 15 μm .

the contrast in MMF. We combine the STABLE and FVM to overcome the mode dispersion and dynamic bending to have high-fidelity donut pattern. Finally, super-resolution imaging under practical movement is achieved.

In the following sections we show the versatility of STABLE in MMF through several demos. In each demonstration, STABLE combines different technical variants to highlight selected imaging effects.

Result

What makes STABLE-based endoscopy compelling is its ability to provide stable imaging under bending, folding and even twisting shapes, without the need to detect or rebuild the distal facet. This makes the

diagnosis more robust and accurate for in vivo imaging inside narrow lumen or in the tissues of solid organs, as desired in clinical applications. We have the MMF with a diverse range of shapes to mimic delicate and difficult-to-reach organs, such as bronchioles and coronary. For each fibre 20–100 deformation states were measured, and we show three deformation states to demonstrate the performance. Detailed information on atherosclerotic and lung cell is preserved well under various shapes (scanning frame rate = 2.5 fps, 96×96 -pixel frame). As shown in Fig. 2d,e and Supplementary Video 1, images can be recovered within about 1 s under operational movements, which includes tracking time, scanning time and synchronization time (as shown in Supplementary Fig. 10). Precalculating and pre-uploading were adopted to eliminate

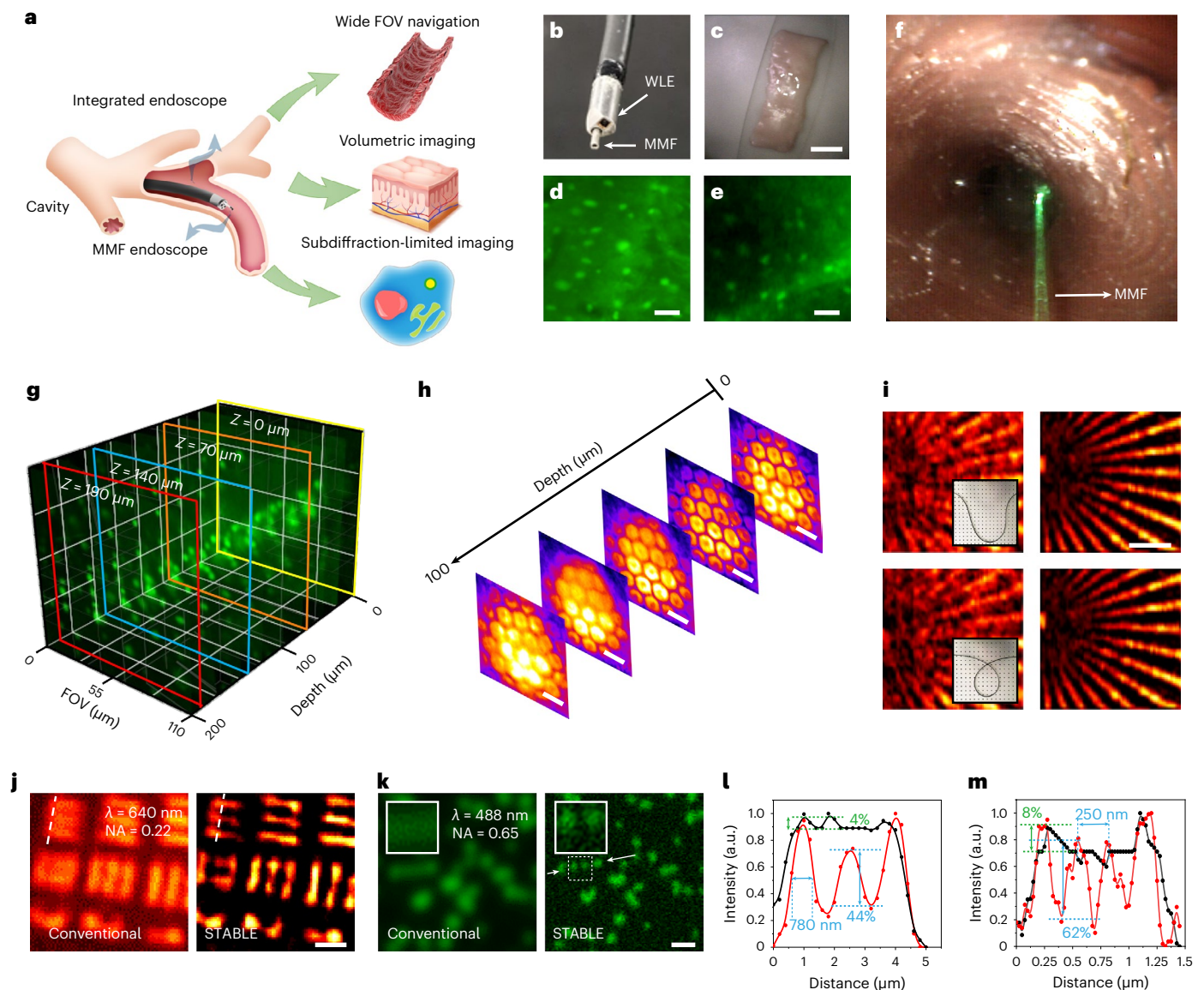


Fig. 4 | Three-dimensional super-resolution imaging and cross-scale imaging characteristics of STABLE endoscopy. **a**, Schematic of STABLE endoscopy for ultrastable slim endoluminal imaging. **b**, The probe of integrated endoscope. **c**, Pig oesophagus imaging through WLE. Scale bar, 1.8 cm. The white dashed box is the observation area for MMF imaging. **d**, Pig oesophagus fluorescence imaging by a wide-field microscope. Scale bar, 25 μm . **e**, Pig oesophagus fluorescence imaging with MMFs. Scale bar, 25 μm . **f**, Wide FOV navigation in the bronchial model. **g**, Fluorescence imaging for a fluorescent microsphere at different focal planes in the glue matrix. Z represents the distance from the end face of the fibre. **h**, Butterfly compound eye was captured at different focal planes. Scale bars, 28 μm . **i**, The deformation state change and super-resolution imaging recovery. The illustrations in the insets represent different fibre

states. The left and right star resolution target images represent the super-resolution imaging without and with STABLE fluorescence emission differences, respectively. Scale bar, 8 μm . **j–m**, Resolution analysis of nano-endoscopy. **j**, Comparisons of the MMF images of a USAF 1951 test target with conventional and STABLE techniques. The resolution of STABLE is 1.5-times improved. Scale bar, 3 μm . **k**, Comparison of the MMF images of fluorescent microsphere with conventional and STABLE techniques. The resolution of STABLE is 1.5-times improved. Scale bar, 0.5 μm . The miniature picture is a local magnified image of the dotted box in the big picture. **l**, Normalized intensity profiles along the white dashed lines in **j**. The solid black curve represents conventional imaging, whereas the solid red curve represents STABLE imaging. **m**, Normalized intensity profiles along lines indicated by the white arrows in **k**.

the calculating and upload time. It should be noticed that in previous studies, the bottleneck for image recovery under dynamic deformation is the slow tracking time (to the order of several minutes). That makes it impossible to recover the image under reasonable movement; complex image recovery has therefore not yet been realized experimentally. The spatial-frequency beacon tracking speeds the tracking time by four orders of magnitude, from several minutes to submilliseconds, offering the ability to track dynamic deformation; however, there still exists other challenges in fast imaging. Synchronization is currently the major limit to recovery, and it can be improved by field programmable gate

array in the future studies. STABLE is also applicable to large bending curvature (Supplementary Video 2). To explore the limit performance of STABLE, we measured the tolerance range of varying the curvature radius and twisting angle (Supplementary Fig. 35); the maximum bending curvature and twisting angle are 80 m^{-1} and 130° , respectively.

To further verify the stability of the proposed scheme over a long time frame, we used STABLE to simultaneously calibrate the optical path drift (Supplementary Note 1) and compensate for disorder. Over a time span of five days, we captured the different areas of the small intestine of a sheep and combined the images captured at different

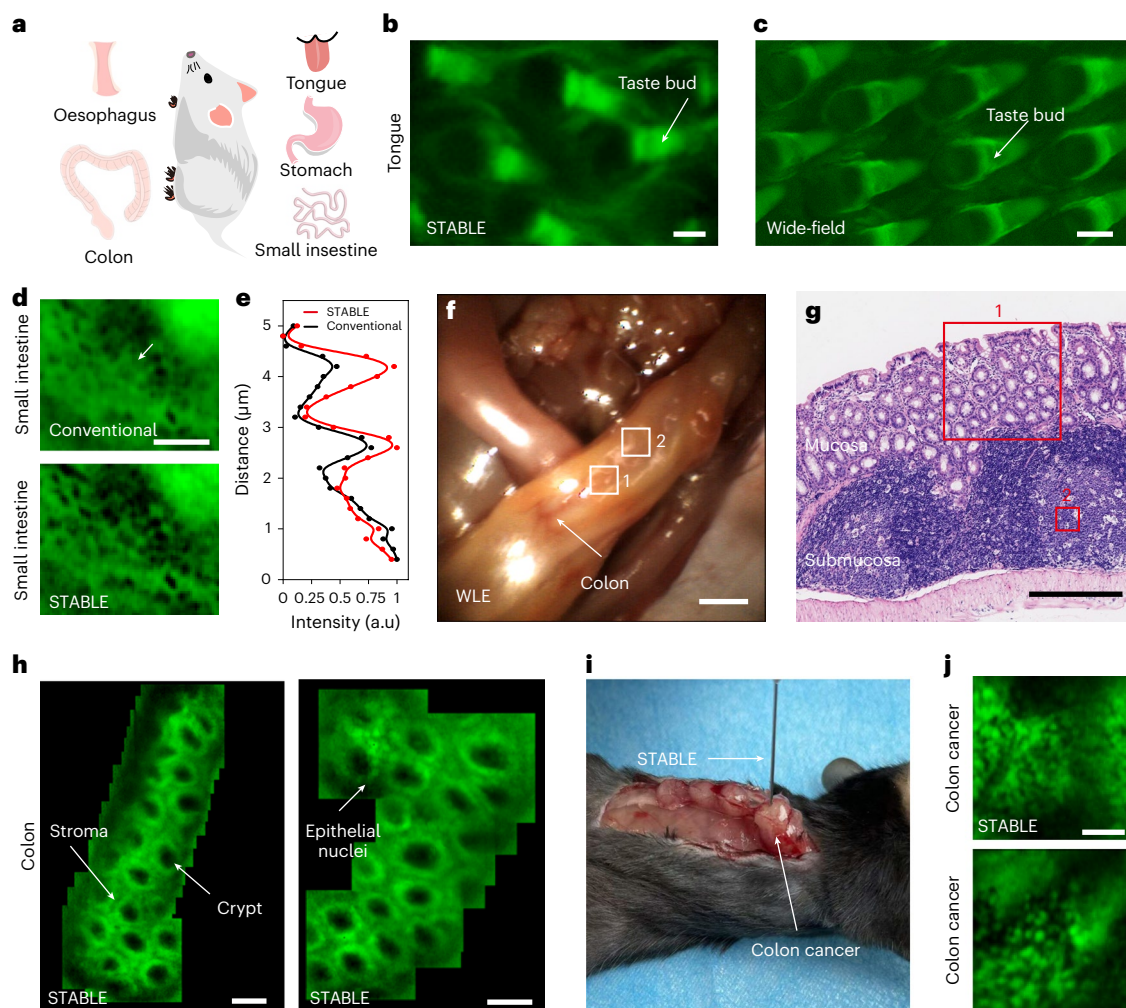


Fig. 5 | STABLE endoscopy for in vivo gastrointestinal imaging. STABLE can provide resolution similar to conventional wide-field microscopy; however, the latter cannot be used in the lumen due to its large size and rigid operation. **a**, Schematic of in vivo imaging. **b, c**, Stitching FOV fluorescence imaging through STABLE endoscopy (**b**) and wide-field microscopy (**c**) at the tongue. Scale bar, 30 μm . **d**, Subdiffraction-limited fluorescence image of the small intestinal mucosa. Scale bar, 5 μm . **e**, Normalized intensity profiles along lines indicated by

white arrow in **d, f**, WLE images showing regions of healthy colon tissue. Scale bar, 4 mm. **g**, Histological sections stained with haematoxylin–eosin from healthy colonic tissue is shown. Scale bar, 300 μm . **h**, Stitching fluorescence image of the healthy colon (regions 1 and 2 in **f**) by STABLE endoscopy. Scale bar, 55 μm . **i**, Colon cancer imaging by STABLE endoscopy. **j**, Fluorescence image of the colon cancer tissue acquired using STABLE endoscopy. Scale bar, 20 μm .

timestamps (Fig. 3b). In a wide FOV image of up to 1 mm (Fig. 3b–d), the goblet cells, absorptive cells and central lacteal were clearly visible. These images are consistent with the conventional wide-field micrographs (Supplementary Fig. 13). For the same focal point, stable focusing was achieved over one week (Fig. 3e), indicating that the system can work stably and consistently in the order of weeks. This aspect is crucial for long-term in situ observations in the life sciences. Moreover, local temperature changes and liquid environments inevitably affect the refractive index of the fibre and cause spherical aberration, which often brings in information distortion. By using STABLE, robust results can be obtained in such complex environments (Fig. 3a). Broad bean anther, onion pollen, basswood segregation and lily pollen were placed underwater to capture clear fluorescent images using a 50 m MMF (Fig. 3j–m). The corresponding wide-field microscope images are shown in Fig. 3f–i. The growth of ice crystals in a capillary was also recorded via MMF imaging (Supplementary Fig. 15). Without the STABLE process, the focal plane shifts rapidly owing to the temperature change at the front of the fibre. This temperature change was well compensated by our STABLE system. The front view of the ice growth inside a 500 μm channel is clearly shown. The observation of ice growth

in capillary may give valuable inspiration in the investigation of plant antifreeze and microchemical reaction.

To validate the stability of the method in long cavity imaging, we used a 200-m-long commercially available MMF to obtain high-contrast projection on an optical table (as shown in Fig. 3n). Using the same optical fibre, we performed fluorescence imaging on a fluorescent lens paper and a CdSe nanowire (Fig. 3o, p). This result showed that STABLE has potential applications that extend from biology to materials science. It should be noted that small fluctuations in the environments will seriously disturb the TM as the fibre length increases. We can have stable imaging under reasonable movement for a fibre length of less than 50 m. When the fibre length is longer than 50 m, STABLE can compensate for the disturbance caused by the environmental fluctuation, but imaging under practical movement has not yet been achieved.

We next performed volumetric imaging of a sample with 5- μm -diameter fluorescent spheres distributed randomly in a glue matrix. A single MMF with a core diameter of 105 μm and a 0.22 NA was used to excite the fluorescent spheres and collect the fluorescence (Fig. 4g). The fluorescent images showed that the spheres could be clearly resolved at imaging depths reaching up to about 200 μm from

the fibre facet (details are given in Supplementary Fig. 20f). Moreover, the structure of the compound eye can be clearly distinguished in the volumetric fluorescence images (Fig. 4h). The proposed method can therefore enable volumetric imaging without mechanical motion.

Based on disorder fast tracking and FVM, spatial-frequency control can then be further used to break the diffraction limit to about $\lambda/3NA$ (Supplementary Note 5). Super-resolution imaging in fibre practical motion is also verified (Fig. 4i). Two samples are used to verify the resolution of STABLE endoscopy (Fig. 4j–m). The intensity profiles along the line indicated by white arrows clearly show 780 nm linewidth in USAF 1951 test target (with $NA = 0.22$ MMF) and 250 nm in fluorescent microspheres sample (with effective $NA = 0.65$ MMF). This implies that the resolution of the STABLE endoscopy is approximately $\lambda/3NA$, which is an improvement of 1.5 times beyond its diffraction limit. Furthermore, axial subdiffraction-limited imaging can be obtained by STABLE (as shown in Supplementary Fig. 27).

Finally, for clinical analysis, localizing a target area in a complex scene is necessary. To bridge the gap between macroscopic and microscopic morphology, wide-FOV and high-resolution 3D imaging capabilities must be combined (Fig. 4a). We integrated the MMF with a self-developed WLE by placing the MMF in the biopsy channel of WLE. An integrated endoscope was used to observe a sample in the bronchus model and pig oesophagus (Supplementary Video 5 and Fig. 4b–f). Fluorescent markers in the outer bottom bronchial tubes were observed synchronously using the MMF and WLE. The WLE offered a wide FOV of approximately 120° , enabling global observation of the oesophagus and bronchus (Supplementary Fig. 16). It also functioned as a guiding tool for the MMF probe toward the diagnosis area. The MMF could thus provide submicrometre 3D imaging of the diagnosis area. The cell is clearly observed in the MMF imaging.

With STABLE, the in vivo high-resolution imaging of the gastrointestinal tracts of mice was first demonstrated for the first time (Fig. 5a). Under the guidance of WLE, MMF ($NA = 0.22$) enables imaging of living cells following spraying topical fluorescent stains inside the tongue, oesophagus, colon, stomach and small intestine (as shown in Fig. 5 and Supplementary Fig. 14). Based on the STABLE, subdiffraction-limited imaging showing different aspects of the small intestinal mucosa is analysed at a subcellular level (Fig. 5d,e). In a healthy colon, epithelial nuclei surround regular, round crypt openings in transepithelial sections (Fig. 5h). Crucially, with subsurface imaging, the spatial resolution degrades due to scattering and aberrations in biological tissues (Supplementary Fig. 29). This impact can be eliminated using MMF as a needle puncture to provide large-depth sampling of the submucosal (Supplementary Fig. 14f and Supplementary Video 6). Compared with those in healthy colonic tissues, the cells are specifically enriched in colon cancer tissue and the crypt structure disappeared (Fig. 5j). They are consistent with histology (Supplementary Fig. 14j,k).

Discussion

Herein we demonstrate a straightforward practical solution for high-resolution micro-endoscopy called STABLE endoscopy, which, based on spatial-frequency-domain coding tracking, can provide scalable bending resistance for most traditional MMF endoscopes without further modification to the fibre. Fundamentally, it solves the general challenge of bending cross-talk in MMF imaging caused by combination of multiple optical physical constraints with simple coding tracking. At present, we can achieve super-resolution imaging under practical movement with a length of less than 50 m. For fibres longer than this, high-resolution imaging was obtained under environmental fluctuations with a fixed position.

As with any imaging system, STABLE imaging involves balancing trade-offs, although it sits on a more optimized trade-off line with a higher performance baseline (Supplementary Note 6). The architecture with the best trade-off should be determined according to specific experimental scenarios. Non-periodic modulation such as

super-pixel-based spatial modulation³⁸ can also be applied with STABLE (Supplementary Fig. 22).

STABLE may also be used in a nonlinear propagation regime for high peak power capable of generating coupling distortions between modes; however, certain problems must be addressed: (1) linear TM cannot describe the relationship between input and output light of MMF in a nonlinear process; and (2) new unstable problems may be caused by nonlinear effects. The STABLE process needs to be modified according to the new approach, which requires further investigation in the future.

Finally, higher super-resolution techniques are worth implementing such as stimulated emission depletion in future systems to further improve image resolution in combination with STABLE. We anticipate that STABLE endoscopy will provide an exciting novel modality for endoscopy widely used in basic and applied research in clinical medicine, biology and industry.

Ethics declarations

All in vivo experiments were approved by the local ethical review committee at the Ethics Committee of the Second Affiliated Hospital of Zhejiang University School of Medicine.

Online content

Any methods, additional references, Nature Portfolio reporting summaries, source data, extended data, supplementary information, acknowledgements, peer review information; details of author contributions and competing interests; and statements of data and code availability are available at <https://doi.org/10.1038/s41566-023-01240-x>.

References

- Mannath, J. & Raganath, K. Role of endoscopy in early oesophageal cancer. *Nat. Rev. Gastroenterol. Hepatol.* **13**, 720–730 (2016).
- Kiesslich, R., Goetz, M., Hoffman, A. & Galle, P. R. New imaging techniques and opportunities in endoscopy. *Nat. Rev. Gastroenterol. Hepatol.* **8**, 547–553 (2011).
- Flusberg, B. A. et al. Fiber-optic fluorescence imaging. *Nat. Methods* **2**, 941–950 (2005).
- Goetz, M., Malek, N. P. & Kiesslich, R. Microscopic imaging in endoscopy: endomicroscopy and endocytoscopy. *Nat. Rev. Gastroenterol. Hepatol.* **11**, 11–18 (2014).
- Orth, A., Plöschner, M., Wilson, E. R., Maksymov, I. S. & Gibson, B. C. Optical fibre bundles: ultra-slim light field imaging probes. *Sci. Adv.* **5**, eaav1555 (2019).
- Buchner, A. M. et al. Comparison of probe-based confocal laser endomicroscopy with virtual chromoendoscopy for classification of colon polyps. *Gastroenterology* **138**, 834–842 (2010).
- Neumann, H. et al. In vivo imaging by endocytoscopy. *Aliment. Pharmacol. Ther.* **33**, 1183–1193 (2011).
- Shin, J. et al. A minimally invasive lens-free computational microendoscope. *Sci. Adv.* **5**, eaaw5595 (2019).
- Hanne, J. et al. STED nanoscopy with fluorescent quantum dots. *Nat. Commun.* **6**, 7127 (2013).
- Li, C. et al. Resolution enhancement and background suppression in optical super-resolution imaging for biological applications. *Laser Photon. Rev.* **15**, 1900084 (2021).
- Sahl, S. J., Hell, S. W. & Jakobs, S. Fluorescence nanoscopy in cell biology. *Nat. Rev. Mol. Cell Biol.* **18**, 685–701 (2017).
- Balzarotti, F. et al. Nanometer resolution imaging and tracking of fluorescent molecules with minimal photon fluxes. *Science* **355**, 606–612 (2017).
- Sigal, Y. M., Zhou, R. & Zhuang, X. Visualizing and discovering cellular structures with super-resolution microscopy. *Science* **361**, 880–887 (2018).

14. Saleh, B. E. A. & Teich, M. C. *Fundamentals of Photonics* (Wiley, 1991).
15. Mahalati, R. N., Gu, R. Y. & Kahn, J. M. Resolution limits for imaging through multi-mode fiber. *Opt. Express* **21**, 1656–1668 (2013).
16. Choi, Y. et al. Scanner-free and wide-field endoscopic imaging by using a single multimode optical fiber. *Phys. Rev. Lett.* **109**, 203901 (2012).
17. Dong, Z. et al. A modulated sparse random matrix for high-resolution and high-speed 3D compressive imaging through a multimode fiber. *Sci. Bull.* **67**, 1224–1228 (2022).
18. Popoff, S. M. et al. Measuring the transmission matrix in optics: an approach to the study and control of light propagation in disordered media. *Phys. Rev. Lett.* **104**, 100601 (2010).
19. Stellinga, D. et al. Time-of-flight 3D imaging through multimode optical fibers. *Science* **374**, 1395–1399 (2021).
20. Plöschner, M., Tyc, T. & Čížmár, T. Seeing through chaos in multimode fibers. *Nat. Photon.* **9**, 529–535 (2015).
21. Leite, I. T. et al. Three-dimensional holographic optical manipulation through a high-numerical-aperture soft-glass multimode fiber. *Nat. Photon.* **12**, 33–39 (2018).
22. Matthès, M. W., Bromberg, Y., de Rosny, J. & Popoff, S. M. Learning and avoiding disorder in multimode fibers. *Phys. Rev. X* **11**, 021060 (2021).
23. Farahi, S., Ziegler, D., Papadopoulos, I. N., Psaltis, D. & Moser, C. Dynamic bending compensation while focusing through a multimode fiber. *Opt. Express* **21**, 22504–22514 (2013).
24. Gordon, G. S. D. et al. Characterizing optical fiber transmission matrices using metasurface reflector stacks for lensless imaging without distal access. *Phys. Rev. X* **9**, 041050 (2019).
25. Vasquez-Lopez, S. A. et al. Subcellular spatial resolution achieved for deep-brain imaging in vivo using a minimally invasive multimode fiber. *Light: Sci. Appl.* **7**, 110 (2018).
26. Papadopoulos, I. N., Farahi, S., Moser, C. & Psaltis, D. High-resolution, lensless endoscope based on digital scanning through a multimode optical fiber. *Biomed. Opt. Express* **4**, 260–270 (2013).
27. Caravaca-Aguirre, A. M. & Piestun, R. Single multimode fiber endoscope. *Opt. Express* **25**, 1656–1665 (2017).
28. Amitonova, L. V. & de Boer, J. F. Endo-microscopy beyond the Abbe and Nyquist limits. *Light Sci. Appl.* **9**, 81 (2020).
29. Wen, Z. et al. Fast volumetric fluorescence imaging with multimode fibers. *Opt. Lett.* **45**, 4931–4934 (2020).
30. Caramazza, P., Moran, O., Murray-Smith, R. & Faccio, D. Transmission of natural scene images through a multimode fibre. *Nat. Commun.* **10**, 2029 (2019).
31. Li, S., Horsley, S. A. R., Tyc, T., Čížmár, T. & Phillips, D. B. Memory effect assisted imaging through multimode optical fibres. *Nat. Commun.* **12**, 3751 (2021).
32. Gu, R. Y., Mahalati, R. N. & Kahn, J. M. Design of flexible multi-mode fiber endoscope. *Opt. Express* **23**, 26905–26918 (2015).
33. Chen, H., Fontaine, N. K., Ryf, R., Neilson, D. T. & Winzer, P. Remote spatio-temporal focusing over multimode fiber enabled by single-ended channel estimation. *IEEE J. Sel. Top. Quantum Electron.* **26**, 1–9 (2020).
34. Xiong, W. et al. Principal modes in multimode fibers: exploring the crossover from weak to strong mode coupling. *Opt. Express* **25**, 2709–2724 (2017).
35. Xiong, W. et al. Complete polarization control in multimode fibers with polarization and mode coupling. *Light Sci. Appl.* **7**, 54 (2018).
36. Anderson, D. Z., Bolshtyansky, M. A. & Zel'dovich, B. Y. Stabilization of the speckle pattern of a multimode fiber undergoing bending. *Opt. Letters* **21**, 785–787 (1996).
37. Rotter, S. & Gigan, S. Light fields in complex media: mesoscopic scattering meets wave control. *Rev. Mod. Phys.* **89**, 015005 (2017).
38. Goorden, S. A., Bertolotti, J. & Mosk, A. P. Superpixel-based spatial amplitude and phase modulation using a digital micromirror device. *Opt. Express* **22**, 17999–18009 (2014).

Publisher's note Springer Nature remains neutral with regard to jurisdictional claims in published maps and institutional affiliations.

Open Access This article is licensed under a Creative Commons Attribution 4.0 International License, which permits use, sharing, adaptation, distribution and reproduction in any medium or format, as long as you give appropriate credit to the original author(s) and the source, provide a link to the Creative Commons license, and indicate if changes were made. The images or other third party material in this article are included in the article's Creative Commons license, unless indicated otherwise in a credit line to the material. If material is not included in the article's Creative Commons license and your intended use is not permitted by statutory regulation or exceeds the permitted use, you will need to obtain permission directly from the copyright holder. To view a copy of this license, visit <http://creativecommons.org/licenses/by/4.0/>.

© The Author(s) 2023

Data availability

The in vivo imaging data underlying this study are available in Figshare with the identifier <https://doi.org/10.6084/m9.figshare.22578691>. Source data are provided with this paper.

Code availability

All codes used to produce the findings of this study are available from the corresponding authors on reasonable request.

Acknowledgements

We acknowledge helpful discussions with Y. Liu, X. Yuan, J. Zhang, Y. Ma, C. Kuang, J. Qi, J. Zhong, J. Xu and Y. Han. Financial support was provided by the National Natural Science Foundation of China (grant nos. T2293751, T2293750, 92250304, 62020106002 and 61735017), National Key Basic Research Program of China (grant no. 2021YFC2401403), Major Scientific Research Project of Zhejiang Laboratory (grant no. 2019MCOAD02) and the Zhejiang University Education Foundation Global Partnership Fund

Author contributions

Q.Y., Z.W. and X.L. conceptualized the work. Q.Y., Z.W. and Z.Y.D. carried out the methodology and investigations. Z.W., Z.Y.D. and J.G.X.

performed visualizations. Q.Y. acquired funding and administered the project. Q.Y., X.L., L.Q.W., J.B.T. and W.C. supervised the work. Z.W. and Q.Y. wrote the original draft, whereas Z.W., Z.Y.D., Q.L.D., C.L.P., Q.Y., X.L., C.F.K. and S.G.L. reviewed and edited it.

Competing interests

The authors declare no competing interests.

Additional information

Supplementary information The online version contains supplementary material available at <https://doi.org/10.1038/s41566-023-01240-x>.

Correspondence and requests for materials should be addressed to Xu Liu or Qing Yang.

Peer review information *Nature Photonics* thanks Vincent Couderc, Christophe Moser and the other, anonymous, reviewer(s) for their contribution to the peer review of this work.

Reprints and permissions information is available at www.nature.com/reprints.